Plasmon enhanced energy-transfer up-conversion in Yb^{3+}- Er^{3+} co-doped $LiNbO_3$ crystal

D. Hernández-Pinilla, P. Molina, J.L Plaza, L.E. Bausá, M.O Ramírez*

Dept. Física de Materiales and Instituto Nicolás Cabrera, Universidad Autónoma de Madrid, Campus de Cantoblanco, 28049-Madrid, Spain

*Corresponding author: mariola.ramirez@uam.es

We have analyzed the effect of linear chains of metallic Ag nanoparticles on the optical properties of a periodically poled Yb^{3+}-Er^{3+} co-doped $LiNbO_3$ crystal. By exploiting the broad plasmonic response supported by linear chains of strongly coupled Ag nanoparticles, we demonstrate a 50% of enhancement of the up-converted Er^{3+} emission under excitation in the *f-f* transition of Yb^{3+} ions. The observed intensification is explained in terms of the broad plasmonic spectral response supported by the Ag chains, which overlaps both the Er^{3+} visible emissions and the Yb^{3+} absorption band, and the two-photon character of the $Yb^{3+} \rightarrow Er^{3+}$ energy-transfer up-conversion process. The results are of interest for applications involving luminescence up-conversion such as sensing, solar energy conversion, biological imaging or solid-state nanolasers.

Keywords

Up-conversion; Yb^{3+}-Er^{3+}:$LiNbO_3$; Plasmon enhancement; Silver nanoparticles chains.

1. Introduction

Nowadays, there is a renewed interest on lanthanide based near infrared (NIR) to visible up-conversion processes due to their applications in a diversity of areas such as biological imaging, sensing, lighting, or renewable energy applications [1-3]. In this respect, Yb^{3+}-Er^{3+} co-doped materials have been extensively studied due to the high absorption cross-section of Yb^{3+} ions at 980 nm and to the efficient $Yb^{3+} \rightarrow Er^{3+}$ energy transfer, which favors the NIR to visible up-conversion processes. However, despite the good performance of the co-doped systems in the NIR region, the visible nonlinear up-converted emission still suffers from low efficiency, which limits its practical implementation. Among the different strategies employed for enhancing up-conversion processes, namely, dopant-host designing [4], core-shell structural engineering [5] or sub-lattice mediated energy clustering [6], the use of plasmonic structures has emerged as a promising strategy. In this sense, the extraordinary capability of metallic nanostructures to confine and enhance the electromagnetic fields at metal-dielectric interfaces can improve both the absorption and the emission involved in the up-conversion processes. In fact, plasmon-enhanced up-converted luminescence has been reported in a variety of architectures including glass composites [7], core-shell nanoparticles [8] or periodically patterned metallic structures [9]. However, little attention has been paid to the effect of plasmonic structures on the up-conversion processes in rare earth (RE) doped single crystals. In previous works, the authors demonstrated the possibility of enhancing the photoluminescence of Nd^{3+} doped $LiNbO_3$ by exploiting the localized surface plasmon (LSP) resonances supported by linear chains of Ag nanoparticles (NPs) deposited on the surface of the crystal [10]. The coupling between the optical transitions of Nd^{3+} and the LSP sustained by the metallic chains resulted in a polarization-dependent enhancement of the Nd^{3+} emission and paved the way for the first demonstration of a RE^{3+} based solid-state laser operating at the subwavelength scale [11]. Thereby, it seems worthwhile to further exploit the interaction between LSP and the optical properties of RE^{3+} doped solid-state crystals to explore the effect of plasmonic structures on the energy transfer up-conversion (ETU) processes involving pairs of optically active RE^{3+} ions.

In this work, we have studied the interaction between the LSPs supported by linear chains of Ag NPs and the $Yb^{3+} \rightarrow Er^{3+}$ ETU emission in $LiNbO_3$. We analyze the influence of the plasmonic structures in both the excitation and the emission and

demonstrate that the visible up-converted emission from Er^{3+} in the proximities of the metallic chains can be enhanced by around 50% when compared to the bare Yb^{3+}-Er^{3+} co-doped $LiNbO_3$ crystal. The observed intensification is explained by considering the spectral response of the LSPs supported by the metallic chains of Ag NPs and the nonlinear character of the $Yb^{3+} \rightarrow Er^{3+}$ ETU process, which involves the participation of two NIR photons resulting in a quadratic boost of the ETU process.

The paper is structured as follows. After describing the fabrication and characterization of the metallic chains of Ag NPs, the effect of the plasmonic structures is evaluated by exciting the system at different wavelengths and analyzing both the one-photon and the two-photon up-converted emissions.

On one side, the possibility of plasmon-enhanced one-photon emission is studied for the green (~550 nm), red (~670 nm) and NIR (~860 nm) transitions of Er^{3+} ions under direct excitation at 488 nm ($^4I_{15/2} \rightarrow {}^4F_{7/2}$ absorption). The effect of the plasmonic structures on the emission of Yb^{3+} ions is also evaluated under direct Yb^{3+} excitation at 920 nm in the NIR region to the $^2F_{7/2}(0) \rightarrow {}^2F_{5/2}(2')$ electronic transition. The experimental results are related to the extinction spectra of the metallic structures.

On the other side, two-photon up-converted emissions of Er^{3+} ions are studied in the proximity of the metallic nanostructures under NIR excitation to Yb^{3+} ions. In this case, the interaction between the LSPs sustained by the metallic arrangements and the $Yb^{3+} \rightarrow Er^{3+}$ ETU photoluminescence produces substantially larger intensification values than those obtained via direct excitation. This behavior can be accounted for in terms of the plasmon-enhanced excitation in the NIR region and in terms of the quadratic character of the NIR to VIS nonlinear process. The results are of interest in the search for improved up-conversion systems operating at the nanoscale and open the way for alternative hybrid plasmonic configurations based on Er^{3+} and Yb^{3+} doped systems.

2. Experimental

2.1 Crystal growth and metallic deposition

An Yb^{3+}-Er^{3+} co-doped $LiNbO_3$ crystal with a periodic structure of alternate ferroelectric domains (PPLN crystal) was growth by the Czochralski off-centered technique along the x-axis. Yb^{3+} and Er^{3+} concentrations relative to Nb^{5+} were found to be 1.30 and 0.03 at %, respectively, as determined by total-reflection x-ray fluorescence

measurements. A 1 mm thick plate was cut and polished up to optical grade with its main faces oriented perpendicular to the ferroelectric *c*-axis (*c*-cut).

The polar surface of the periodically poled Yb^{3+}-Er^{3+}:$LiNbO_3$ crystal was used as a platform for polarization mediated chemistry enabling an easy-to-apply, scalable and effective cost method for the deposition of metallic nanoparticles [12]. By means of a photochemical procedure, linear chains of Ag NPs were obtained on the surfaces of the domain boundaries of the $LiNbO_3$ crystal. See details elsewhere [10]. Nanometric-scaled images of the metallic array structures were obtained by a scanning electron microscope (SEM) model Philips XL30 SFEG. The NPs exhibit a nearly spherical shape with an average diameter close to 50 nm. The interspacing distance of the nanoparticles forming the chains was less than 5 nm.

2.2 Optical characterization

The extinction spectrum of the hybrid Yb^{3+}-Er^{3+}:$LiNbO_3$-plasmonic system was obtained in transmission mode by using a Lambda 1050 Perkin Elmer spectrophotometer. A laser scanning confocal microscope (Olympus BX41) provided with a software controlled two-axis XY motorized platform with 0.2 μm spatial resolution was used to obtain the micro-luminescence spectra. An Ar^+ laser tuned at 488 and a cw Ti:Sapphire laser (Spectra Physics Model 177-Series) were used as excitation sources. The excitation beam was focused on the surface of the crystal by a 100x microscope objective. The same objective was used to collect the photoluminescence signal from the crystal in backscattering geometry. A Peltier-cooled Horiba Synapse CCD was used for the detection. The experiments were carried out at room temperature.

3. Results and discussion

The plasmonic geometries employed for boosting the up-converted emission can be classified into two main groups depending on the spectral range of the LSP and that of the involved RE^{3+} transitions: i) LSP overlapping the RE^{3+} absorption transition or ii) LSP overlapping the spectral region of the emission transition. Such distinction is relevant since, in general, the large spectral shift between the absorption, in the NIR, and the visible up-converted emissions, prevents the simultaneous spectral overlap of the LSP with the excitation and emission channels. In fact, most of the published works on this topic use plasmonic architectures with their resonance centered in the visible

range, according to the LSP resonances of the employed plasmonic structures, (isolated silver or gold nanoparticles). In this case, the plasmonic nano-antennas enhance the radiative emission rate of the spectrally overlapped transition through the Purcell effect [13,14]. On the other hand, the enhancement of the excitation radiation due to spectral overlap between the LSP resonance and the NIR absorption can take advantage of the quadratic dependence of the up-converted emissions on the excitation to improve the response of the system. Further, it would allow the simultaneous enhancement of all the up-conversion emission bands regardless their spectral emission location. However, the number of plasmonic structures fabricated to this end is very scarce and it has been mainly focused on metallic structures supporting propagating surface plasmon polaritons [9,15].

An interesting approach to extend the LSP resonance sustained by metallic nanostructures to a broad spectral range relies on the excitation of collective modes supported by arrangements of closely spaced interacting metallic nanoparticles. In the present work we have used linear chains of strongly coupled Ag NPs as plasmonic arrangements for enhancing the ETU process.

Fig. 1(a) shows the typical experimental extinction spectrum associated with long linear chains (millimeter length) of nearly spherical Ag NPs with an average size of 50 nm and interspacing distances of few nanometers (< 5nm) photo-deposited on the surfaces of domain boundaries of the *c*-cut PPLN crystal. The inset shows a representative SEM image of a portion of a metallic chain. The spectrum was obtained in transmission mode after subtracting the spectrum associated to the bare (non-metalized) RE^{3+} doped $LiNbO_3$ crystal. As seen, the Ag NP chains exhibit a broad spectral response with a maximum at around 600 nm and a long decreasing tail which extends to wavelength values beyond 1 μm. The spectral shape correlates well with the theoretical simulations of the optical response of the chains [16], the large bandwidth being related to the distribution of sizes and interparticle distances of the Ag NPs forming the plasmonic chains. This extinction spectrum overlaps the absorption and emission spectra of the Er^{3+} and Yb^{3+} ions in the visible and NIR spectral region, and provides an exceptional scenario for studying the plasmon-enhanced absorption and fluorescence under different excitation wavelengths. Fig. 1(b) shows the emission spectra analyzed in this work. They involved different optical transitions of Yb^{3+} and Er^{3+} ions in $LiNbO_3$. In particular, the bands centered at around 550, 670 and 860 nm which correspond to the $^4S_{3/2} + ^2H_{11/2} \rightarrow {}^4I_{15/2}$, $^4F_{9/2} \rightarrow {}^4I_{15/2}$ and $^4S_{3/2} + ^2H_{11/2} \rightarrow {}^4I_{13/2}$ transitions of Er^{3+} ions,

respectively. These transitions are accessible via direct excitation or via $Yb^{3+} \rightarrow Er^{3+}$ ETU process. The emission band centered at 1μm related to the $^2F_{5/2} \rightarrow {}^2F_{7/2}$ radiative de-excitation of Yb^{3+} ions in $LiNbO_3$ is also shown. For the sake of comparison, the relative contribution of the different Er^{3+} transitions has been normalized to the maximum of the emission spectrum of Yb^{3+}. As observed, most up-converted emission bands spectrally overlap the extinction spectrum of the Ag NPs chains, as well as the Yb^{3+} absorption and emission transitions in the NIR region ($\lambda \sim 1$ μm).

Once the overlap between the LSP and the optical transitions involved in the up-conversion processes is evidenced, the optical behavior of the hybrid Yb^{3+}-Er^{3+}:$LiNbO_3$-plasmonic system is studied by using spatially resolved confocal spectroscopy.

3.1 Single photon process

Fig. 2(a) shows the micro-fluorescence spatial map obtained by integrating the Er^{3+} $^4S_{3/2} + {}^2H_{11/2} \rightarrow {}^4I_{15/2}$ emission (520-560 nm green spectral region) under direct excitation at 488 nm in the vicinities of an Ag NPs chain. The SEM image of the corresponding plasmonic chain is also shown. As seen, a clear enhancement of the emission in the proximities of the plasmonic arrangement is observed. Similar results are obtained when analyzing the integrated emission associated with the $^4F_{9/2} \rightarrow {}^4I_{15/2}$ (red) and $^4S_{3/2} + {}^2H_{11/2} \rightarrow {}^4I_{13/2}$ (NIR) emission transitions of Er^{3+} ions.

Here it is worth mentioning that similar spectroscopic imaging experiments on the same Yb^{3+}-Er^{3+}:$LiNbO_3$ sample, but in absence of metallic nanoparticles, results into a flat contour fluorescence map. Therefore the possible impact of slight compositional variations in our crystal can be neglected.

Fig. 2(b-d) show the comparison between the emission spectra collected in and out of the vicinity of the Ag NPs chain in different spectral regions. The spectra show a well resolved structure consistent with the Stark splitting of the involved states by the effect of the crystal field. The number of transitions and their relative intensities are also in agreement with previous works [17]. The comparison shown in Fig. 2 reveals two main features: i) the interaction between the LSP and the optical transitions of Er^{3+} produces an intensification of the emitted intensity in the vicinity of the metallic arrangements, but the spectral shape is not modified. This indicates that the forced electric-dipole character of the transitions is not altered by the plasmonic structures; ii) the

intensification factor of the emissions (obtained as the ratio between the integrated intensities in and out of the vicinity of the plasmonic structures) shows similar values, around 20%, regardless of the spectral region. Therefore, even if an enhancement of the radiative emission rate cannot be ruled out, the obtained results suggest the enhancement of the electric field of the incident light, which leads to the enhancement of the absorption transition at 488 nm, as a dominant mechanism for the observed photoluminescence intensification.

We would like to mention that mapping the intensity ratio between the $^2H_{11/2} \rightarrow {}^4I_{15/2}$ (~ 520 nm) and $^4S_{3/2} \rightarrow {}^4I_{15/2}$ (~ 550 nm) emissions of Er^{3+} ions results into a featureless image in the proximities of the Ag NPs chain. Therefore, according to the great sensitivity to thermal effects of the green emissions of Er^{3+} [18,19], a plasmonic driven thermal heating effect can be neglected in our system. This is in agreement with the dominant radiative character of the broad plasmonic mode centered at 600 nm supported by the metallic chains of NPs [20].

3.2 Two-photon process

Fig. 3 shows the emission spectra recorded in and out the vicinity of the metallic chains under excitation in the NIR region. In this case, the participation of Yb^{3+} ions has been involved in the process by fixing the excitation wavelength at 920 nm, which corresponds to the $^2F_{7/2}(0) \rightarrow {}^2F_{5/2}(2')$ Yb^{3+}electronic transition in $LiNbO_3$ [21]. As it is well known, in Yb^{3+}-Er^{3+} co-doped systems, once the $^2F_{5/2}$ excited state of Yb^{3+} ions has been populated it may either decay radiatively to its fundamental state emitting one photon in the 900-1100 nm spectral range, or transfer its energy to Er^{3+} ions via a cross relaxation mechanism. A schematics of the resonant energy transfer mechanism involving the $^4I_{11/2}$ (Er^{3+}) level, together with the main up-conversion processes, and the monitored visible emissions, has been depicted in Fig. 3(a). A detailed analysis of the energy transfer mechanisms in Yb^{3+}-Er^{3+}:$LiNbO_3$ can be found elsewhere [22,23].

Fig. 3(b) shows the influence of the metallic nanostructures on the $^2F_{5/2}(0') \rightarrow {}^2F_{7/2}(0)$ emission transition of Yb^{3+} ions. As seen, the Yb^{3+} photoluminescence is enhanced by the Ag NPs chain under direct excitation in the NIR. Nevertheless, the obtained intensification factor is lower than the obtained for Er^{3+} emissions when pumping at 488 nm ($^4I_{15/2} \rightarrow {}^4F_{7/2}$ optical transition of Er^{3+}) (roughly half the value), in agreement with the lower extinction values sustained by the metallic chains at longer wavelengths (see Fig. 1(a)).

Fig. 3(c) and (d) show the green and red up-converted emissions, respectively, obtained in and out of the vicinity of Ag NPs chains. As expected, the spectral shape is similar to that obtained under direct excitation (see Fig. 2(b-c)). However, they show a substantially higher intensification factor, near 50%, when excited via $Yb^{3+} \rightarrow Er^{3+}$ resonant energy transfer. The different enhancement observed can be associated with the nonlinear character of the up-conversion process which involves the participation of two NIR photons. In fact, in the weak excitation regime, the up-converted emission enhancement results much larger than the observed for the one-photon emission due to its quadratic dependence on the field enhancement at the NIR excitation wavelength. As a consequence, a much higher intensification is obtained even though the extinction values are larger in the visible spectral region. The obtained results are in agreement with previous reports on the behavior of the enhancement of the up-converted visible radiation by quadratic second harmonic generation processes, where the key role of plasmon enhancing the fundamental radiation was highlighted [24]. The work points out the potential of chains of interacting nanoparticles for enhancing the nonlinear optical response of the system via the intensification of the excitation radiation at the near infrared region, and provides a new approach for the development of efficient nonlinear photonic devices at the nanoscale.

4. Summary and Conclusions

To summarize, we have analyzed the interaction between the LSP resonance supported by linear chains of Ag NPs on the optical properties of a periodically poled Yb^{3+}-Er^{3+} co-doped $LiNbO_3$ crystal. The plasmonic arrangements were obtained by means of a cost effective photo-chemical procedure using the ferroelectric domain structure of a PPLN crystal as template for the NPs chain formation on the domain walls. The collective dipole modes supported by the metallic chains result into a broad plasmonic resonance which spectrally overlap with both the Er^{3+} visible emissions and the Yb^{3+} absorption in the near infrared region. This fact has been exploited to demonstrate the possibility of plasmon-enhanced one-photon emission for both, Er^{3+} and Yb^{3+} ions. Further, we show the possibility to enhance the Er^{3+} up converted luminescence via $Yb^{3+} \rightarrow Er^{3+}$ energy transfer up to 50%, due to the two-photon character of the process. To our knowledge, this constitutes the first study on the impact of LSP on up-converted luminescence using a bulk single crystal as optically active substrate for plasmonic nanostructures. The results provide an alternative approach to the expanding field of

plasmon-enhanced up-converted luminescence and open the way for novel hybrid plasmonic configurations based on different noble metal arrangements.

5. Acknowledgements

This work has been supported by the Spanish Ministry of Economy and Competitiveness (MINECO) under project MAT2013-43301-R and Comunidad de Madrid under grant S2013/MIT-2740.

References

[1] S. H. Nam, Y. M. Bae, Y. I. Park, J. H. Kim, H. M. Kim, J. S. Choi, K. T. Lee, T. Hyeon, Y. D. Suh, Long-term real-time tracking of lanthanide ion doped upconverting nanoparticles in living cells, Angew. Chem. Int. Ed. 50 (2011) 6093-6097.

[2] V. Kumar Rai, A. Pandey, R. Dey, Photoluminescence study of Y_2O_3:Er^{3+}-Eu^{3+}-Yb^{3+} phosphor for lighting and sensing applications, J. Appl. Phys. 113 (2013) 083104.

[3] T. Trupke, M. A. Green, P. Würfel, Improving solar cell efficiencies by up-conversion of sub-band-gap light, J. Appl. Phys. 92 (2002) 4117-4122.

[4] X. Li, F. Zhang, D. Zhao, Lab on upconversion nanoparticles: Optical properties and applications engineering via designed nanostructure, Chem. Soc. Rev. 44 (2015) 1346-1378.

[5] F. Wang, R. Deng, J. Wang, Q. Wang, Y. Han, H. Zhu, X. Chen, X. Liu, Tuning upconversion through energy migration in core–shell nanoparticles, Nat. Mater. 10 (2011) 968-973.

[6] J. Wang, R. Deng, M. A. MacDonald, B. Chen, J. Yuan, F. Wang, D. Chi, T. S. Andy Hor, P. Zhang, G. Liu, Y. Han, X. Liu, Enhancing multiphoton upconversion through energy clustering at sublattice level, Nat. Mater. 13 (2014) 157-162.

[7] D. M. da Silva, L. R. P. Kassab, S. R. Lüthi, C. B. de Araújo, A. S. L. Gomes, M. J. V. Bell, Frequency upconversion in Er^{3+} doped PbO–GeO_2 glasses containing metallic nanoparticles, Appl. Phys. Lett. 90 (2007) 081913.

[8] P. Yuan, Y. H. Lee, M. K. Gnanasammandhan, Z. Guan, Y. Zhang, Q.-H. Xu, Plasmon enhanced upconversion luminescence of $NaYF_4$:Yb,Er@SiO_2@Ag core-shell nanocomposites for cell imaging, Nanoscale 4 (2012) 5132-5137.

[9] D. Lu, S. K. Cho, S. Ahn, L. Brun, C. J. Summers, W. Park, Plasmon enhancement mechanism for the upconversion processes in $NaYF_4$:Yb^{3+},Er^{3+} nanoparticles: Maxwell versus Förster, ACS Nano 8 (2014) 7780-7792.

[10] E. Yraola, P. Molina, J. L. Plaza, M. O Ramírez, L. E. Bausá, Spontaneous emission and nonlinear response enhancement by silver nanoparticles in a Nd^{3+}-doped periodically poled $LiNbO_3$ laser crystal, Adv. Mater. 25 (2013) 910-915.

[11] P. Molina, E. Yraola, M. O Ramírez, C. Tserkezis, J. L. Plaza, J. Aizpurua, J. Bravo-Abad, L. E. Bausá, Plasmon-assisted Nd^{3+}-based solid-state nanolaser, Nano Lett. 16 (2016) 895-899.

[12] S. V. Kalinin, D. A. Bonnell, T. Alvarez, X. Lei, Z. Hu, R. Shao, J. H. Ferris, Ferroelectric lithography of multicomponent nanostructures, Adv. Mater. 16 (2004) 795-799.

[13] W. Park, D. Lu, S. Ahn, Plasmon enhancement of luminescence upconversion, Chem. Soc. Rev. 44 (2015) 2940-2962.

[14] D. M. Wu, A. García-Etxarri, A. Salleo, J. A. Dionne, Plasmon-Enhanced Upconversion, J. Phys. Chem. Lett. 5 (2014), 4020-4031.

[15] Q. C. Sun, H. Mundoor, J. C. Ribot, V. Singh, I. I. Smalyukh, P. Nagpal, Plasmon-enhanced energy transfer for improved upconversion of infrared radiation in doped-lanthanide nanocrystals, Nano Lett. 14 (2014) 101-106.

[16] E. Yraola, L. Sánchez-García, C. Tserkezis, P. Molina, M. O Ramírez, J. Aizpurua, L. E. Bausá, Polarization-selective enhancement of Nd^{3+} photoluminescence assisted by linear chains of silver nanoparticles, J. Lumin. 169 Part B (2016) 569-573.

[17] L. Núñez, G. Lifante, F. Cussó, Polarization effects on the line-strength calculations of Er^{3+}-doped $LiNbO_3$, Appl. Phys. B 62 (1996) 485-491.

[18] M. Quintanilla, E. Cantelar, F. Cussó, M. Villena, A. C. Caballero, Temperature sensing with up-converting submicron-sized $LiNbO_3$:Er^{3+}/Yb^{3+} particles, Appl. Phys. Express 4 (2011) 022601.

[19] S. F. León-Luis, U. R. Rodríguez-Mendoza, P. Haro-González, I. R. Martín, V. Lavín, Role of the host matrix on the thermal sensitivity of Er^{3+} luminescence in optical temperature sensors, Sens. Actuators B-Chem. 174 (2012) 176-186.

[20] E. Yraola, L. Sánchez-García, C. Tserkezis, P. Molina, M. O Ramírez, J. L. Plaza, J. Aizpurua, L. E. Bausá, Controlling solid state gain media by deposition of silver nanoparticles: From thermally-quenched to plasmon-enhanced Nd^{3+} luminescence, Opt. Express 23 (2015) 15670-15679.

[21] E. Montoya, A. Lorenzo, L. E. Bausá, Optical characterization of $LiNbO_3$:Yb^{3+} crystals, J. Phys.: Condens. Matter 11 (1999) 311-320.

[22] E. Cantelar, J. A. Muñoz, J. A. Sanz-García, F. Cussó, Yb^{3+} to Er^{3+} energy transfer in $LiNbO_3$, J. Phys.: Condens. Matter 10 (1998) 8893-8903.

[23] E. Cantelar, F. Cussó, Dynamics of the Yb^{3+} to Er^{3+} energy transfer in $LiNbO_3$, Appl. Phys. B 69 (1999) 29-33.

[24] L. Sánchez-García, C. Tserkezis, M.O Ramírez, P. Molina, J.J. Carvajal, M. Aguiló, F. Díaz, J. Aizpurua, L. E. Bausá, Plasmonic enhancement of second harmonic generation from nonlinear $RbTiOPO_4$ crystals by aggregates of silver nanostructures,

Opt. Express 24 (2016) 8491-8500.

FIGURE CAPTIONS

Figure 1.- Extinction spectrum associated with linear chains of Ag NPs with an average size of 50 nm deposited on the surface of $LiNbO_3$ crystal. The inset shows a representative SEM image of a single Ag NP chain photo-chemically formed on the surface of a domain boundary. The arrows on the spectrum indicate the two different excitation wavelengths used in this work: 488 nm related to the $^4I_{15/2} \rightarrow {}^4S_{3/2} + {}^2H_{11/2}$ absorption of Er^{3+} ions, and 920 nm related to the $^2F_{7/2} \rightarrow {}^2F_{5/2}$ absorption of Yb^{3+} ions. b) Experimentally obtained emission spectra of the $^4S_{3/2} + {}^2H_{11/2} \rightarrow {}^4I_{15/2}$ (green), $^4F_{9/2} \rightarrow {}^4I_{15/2}$ (red) and $^4F_{9/2} \rightarrow {}^4I_{13/2}$ (dark red) transitions of Er^{3+} ions in $LiNbO_3$. The $^2F_{5/2} \rightarrow {}^2F_{7/2}$ (black) emission of Yb^{3+} ions is also shown. For illustrative purposes, the Er^{3+} green emission and the Yb^{3+} emission spectra have been normalized.

Figure 2.- Intensification of the photoluminescence of Er^{3+} ions in the proximities of a single Ag NPs chain under excitation at 488 nm. a) SEM image of the Ag NPs chain (left) and micro-fluorescence spatial map obtained by integrating the $^4S_{3/2} + {}^2H_{11/2} \rightarrow {}^4I_{15/2}$ transition of Er^{3+} in the surroundings of the Ag NPs chains (right). The yellow zones in the map corresponds to the highest intensity. b-d) Emission spectra associated with the $^4S_{3/2} + {}^2H_{11/2} \rightarrow {}^4I_{15/2}$, $^4F_{9/2} \rightarrow {}^4I_{15/2}$ and $^4F_{9/2} \rightarrow {}^4I_{13/2}$ transitions of Er^{3+} under direct excitation at 488 nm. The emission spectra obtained in (red lines) and out (blue lines) of the vicinity of the plasmonic chains (red lines) are compared. Enhancement factors due to the presence of the plasmonic chains of Ag NPs are shown in each case.

Figure 3.- a) Schematics of the resonant energy transfer mechanism involving the $^4I_{11/2}$ (Er^{3+}) level, together with the main up-conversion processes, and the monitored visible emissions. Emission spectra associated with the b) $^2F_{5/2} \rightarrow {}^2F_{7/2}$ transition of Yb^{3+}; c) $^4S_{3/2} + {}^2H_{11/2} \rightarrow {}^4I_{15/2}$, and d) $^4F_{9/2} \rightarrow {}^4I_{15/2}$ and $^4F_{9/2} \rightarrow {}^4I_{13/2}$ transitions of Er^{3+} under excitation at 920 nm. The emission spectra obtained in (red lines) and out (blue lines) of the vicinity of the plasmonic chains are compared. Enhancement factors due to the presence of the plasmonic chains of Ag NPs are shown in each case.

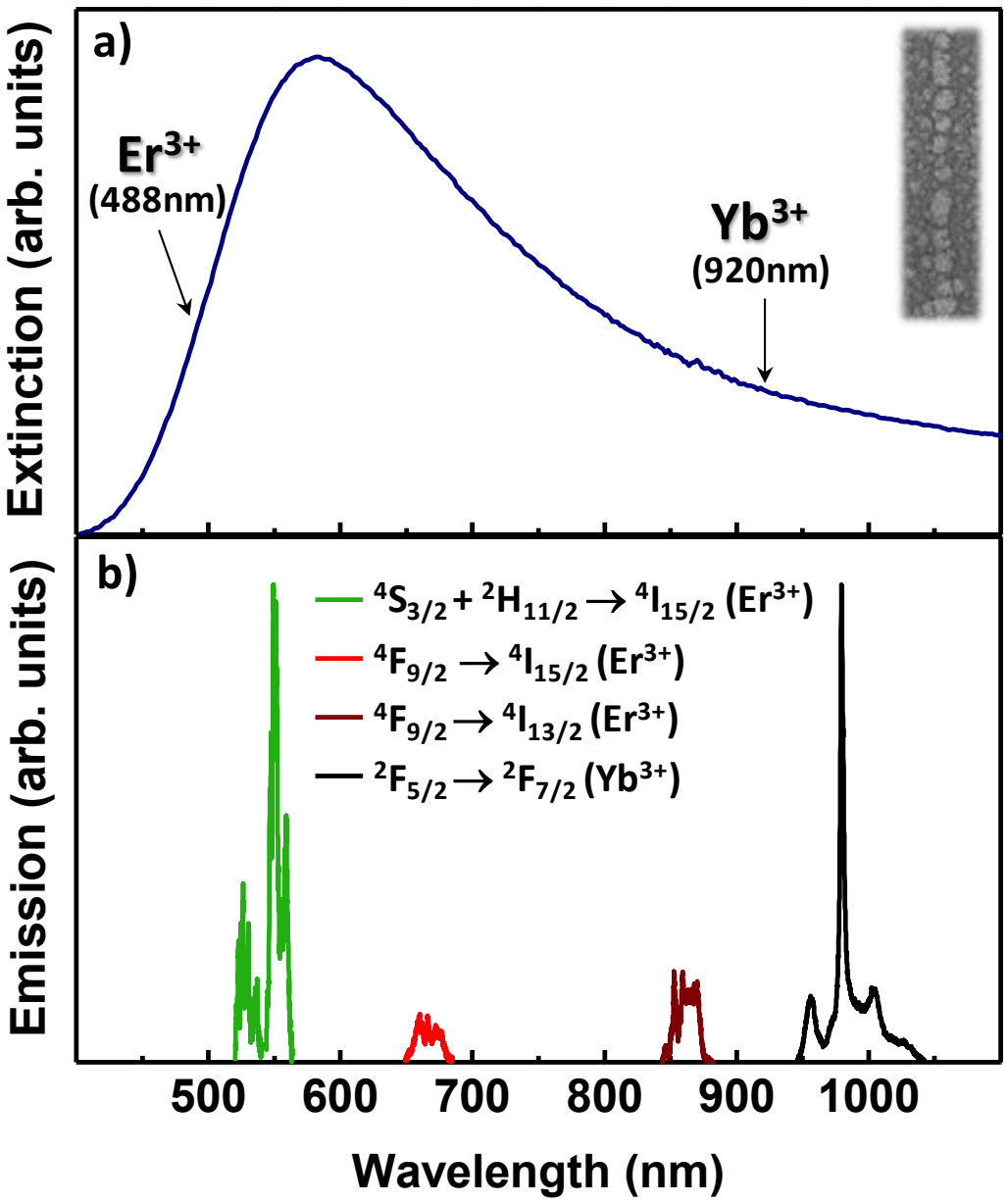
a)
Er3+
(488nm)
Yb3+
(920nm)
Extinction (arb. units)
b)
4S3/2 + 2H11/2 → 4I15/2 (Er3+)
4F9/2 → 4I15/2 (Er3+)
4F9/2 → 4I13/2 (Er3+)
2F5/2 → 2F7/2 (Yb3+)
Emission (arb. units)
500
600
700
800
900
1000
Wavelength (nm)

Figure 1

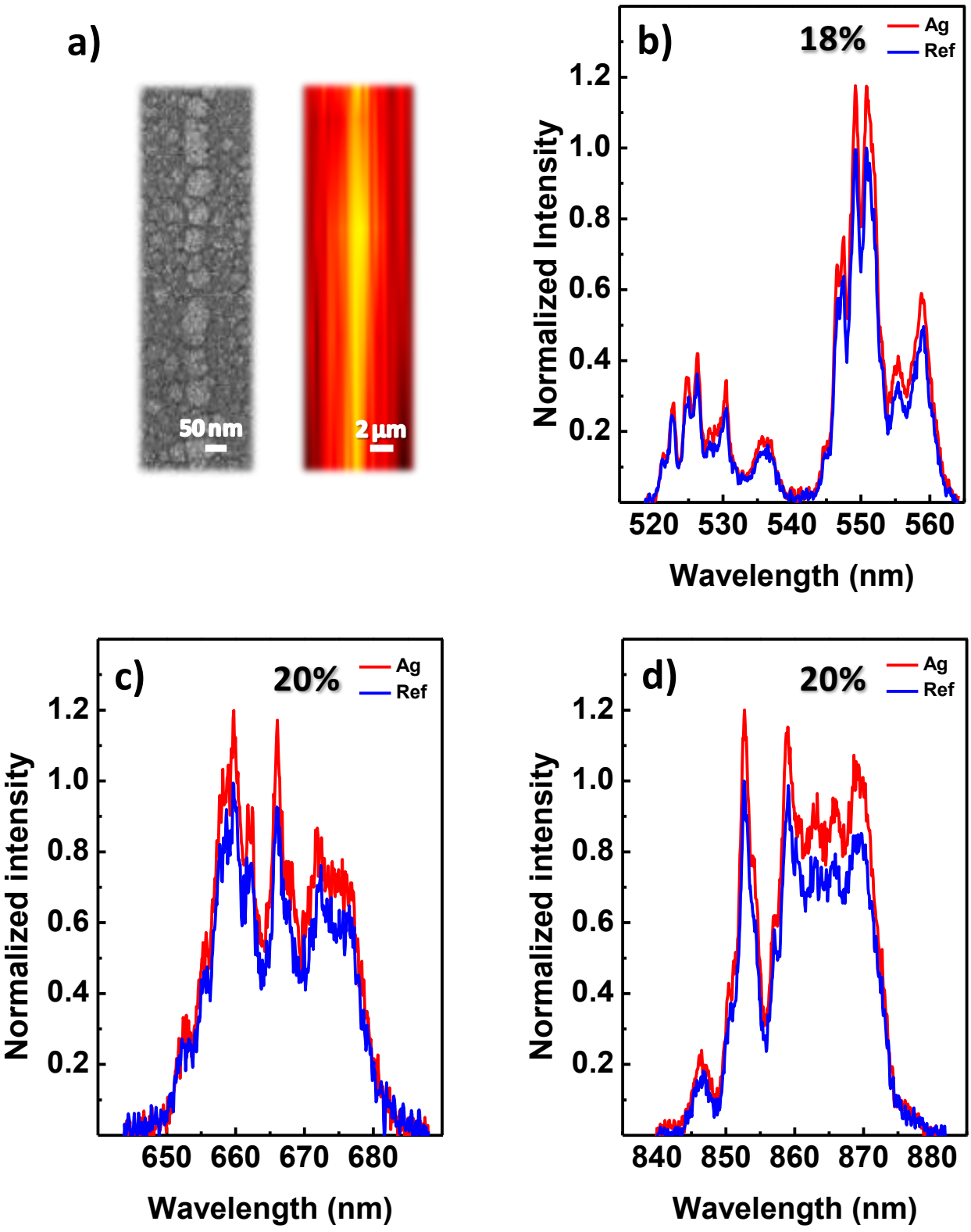
a)
50 nm
2 µm
b)
18%
Ag
Ref
Normalized Intensity
1.2
1.0
0.8
0.6
0.4
0.2
520 530 540 550 560
Wavelength (nm)
c)
20%
Ag
Ref
Normalized intensity
1.2
1.0
0.8
0.6
0.4
0.2
650 660 670 680
Wavelength (nm)
d)
20%
Ag
Ref
Normalized intensity
1.2
1.0
0.8
0.6
0.4
0.2
840 850 860 870 880
Wavelength (nm)

Figure 2

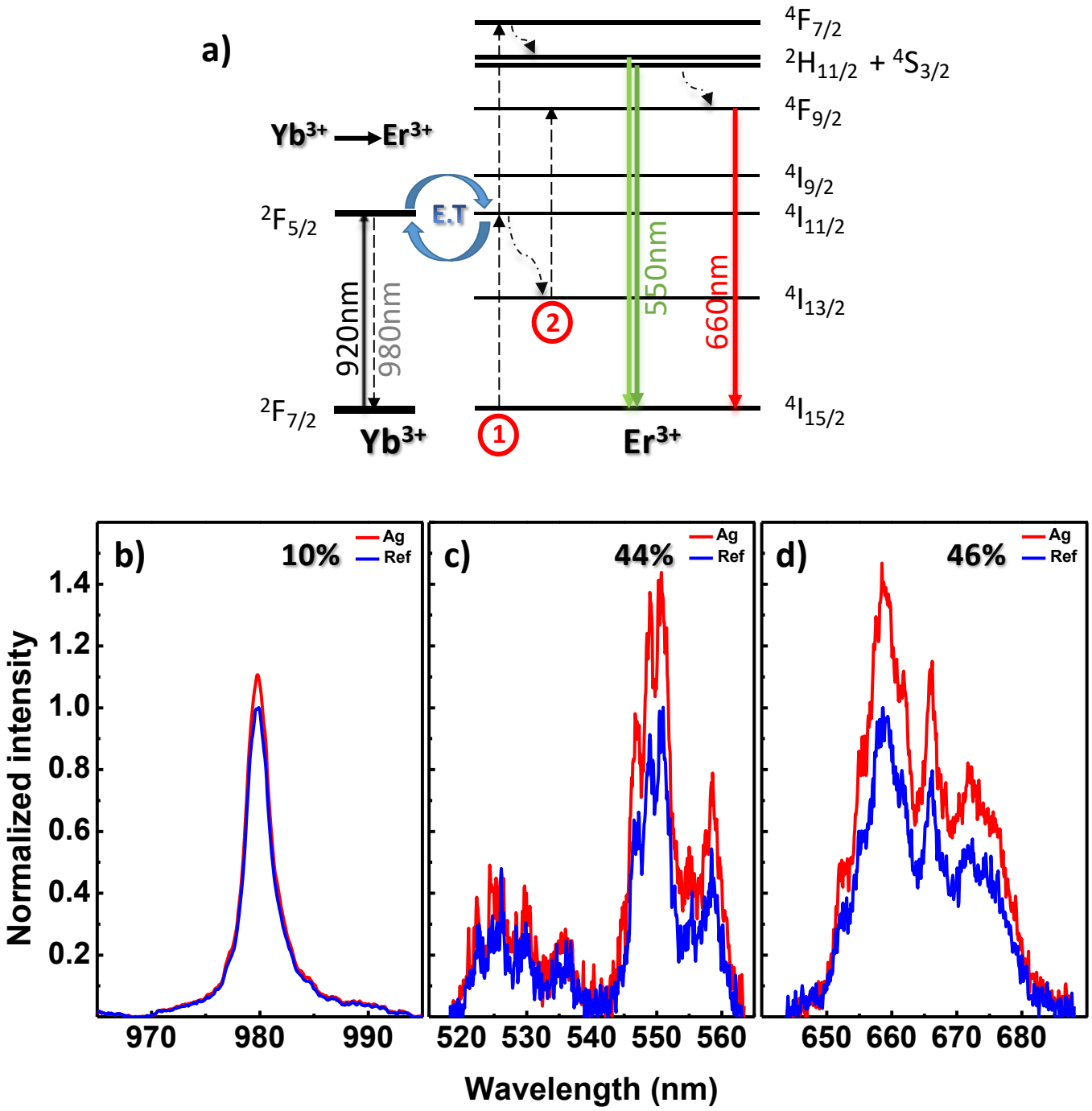
a)
Yb3+ → Er3+
E.T
2F5/2
2F7/2
920nm
980nm
4F7/2
2H11/2 + 4S3/2
4F9/2
4I9/2
4I11/2
4I13/2
4I15/2
550nm
660nm
1
2
Yb3+
Er3+
b)
10%
Ag
Ref
c)
44%
Ag
Ref
d)
46%
Ag
Ref
Normalized intensity
1.4
1.2
1.0
0.8
0.6
0.4
0.2
970
980
990
520
530
540
550
560
650
660
670
680
Wavelength (nm)

Figure 3